

Evaluating Site Amplification Factor of Response Spectrum Using Microtremor Horizontal-to-Vertical Spectral Ratio

Ruibin Wang^{*,‡}, Haizhong Zhang^{†,§} and Yan-Gang Zhao^{*,¶}

**Key Laboratory of Urban Security
and Disaster Engineering of Ministry of Education
Beijing University of Technology*

No. 100, Pingleyuan, Chaoyang, Beijing 100124, P. R. China

*†Faculty of Agriculture, Yamagata University
1-23, Wakaba-machi, Tsuruoka-shi, Yamagata 997-8555, Japan*

‡wrb12370@163.com

§zhang@tds1.tr.yamagata-u.ac.jp

¶zhaoyg@bjut.edu.cn

Received 14 September 2024

Revised 4 April 2025

Accepted 4 April 2025

Published 29 May 2025

Site amplification factor of response spectrum (SAFRS) plays a crucial role in seismic design. Existing methods for evaluating SAFRS typically require site-specific information, such as soil layer thickness and shear wave velocity. However, obtaining this information often necessitates drilling, which is both complex and costly. To avoid using such site information, this study aims to propose a method for evaluating SAFRS using the microtremor horizontal-to-vertical spectral ratio (MHVSR). To this end, first, a formula is developed to calculate SAFRS at the site fundamental period using MHVSR based on an analysis of microtremor data and site response results from 42 sites in Yokohama, Japan. In addition, to account for nonlinear site effects on SAFRS, formulae are derived to estimate the variation rates of the site fundamental period and SAFRS at the site fundamental period with changes in ground motion intensity. Furthermore, by combining a SAFRS model for various periods from previous research, SAFRS at various periods are calculated based on the site fundamental period and SAFRS at the site fundamental period. Finally, the proposed method is validated through linear and nonlinear site response analyses.

Keywords: Site amplification factor of response spectrum; microtremor horizontal-to-vertical spectral ratio; the site fundamental period.

1. Introduction

Site effects have been widely studied due to their significant impact on ground motion characteristics [Morikawa and Iiyama, 2021; Baoyintu and Kawase, 2021;

§Corresponding author.

Zhang and Zhao, 2021b; Shi *et al.*, 2022a; Liu *et al.*, 2022; Parla and Somala, 2022; Isari *et al.*, 2023; Yu *et al.*, 2023; Li *et al.*, 2024; Liu and Li, 2024; Phung *et al.*, 2024; Karimzadeh and Askan Gündoğan, 2024; Bozdogan and Keskin, 2024; Wen *et al.*, 2024; Wen and Bi, 2025]. Since the 1970s, seismic design codes in many countries have progressively incorporated site amplification effects into the design response spectrum, such as the Chinese seismic code [GB 50011, 2010], the American seismic code [IBC, 2012; ASCE/SEI 7-10, 2010], and the Japanese seismic code [Midorikawa *et al.*, 2003]. Site amplification factor of response spectrum (SAFRS) is widely used to describe site amplification effects and is defined as the ratio of the soil-surface response spectrum to the bedrock response spectrum.

Numerous methods have been proposed to calculate SAFRS. Borchardt [1994] and Dobry *et al.* [2000] derived formulae for calculating SAFRS at long and short periods based on borehole data, strong-motion data, and numerical modeling results. Lam *et al.* [2001] introduced a method to determine SAFRS at the site fundamental period, RF_{T_1} , by simulating soil vibrational behavior through the vibrational analysis of a multi-storey moment-resisting frame with rigid girders. Tsang *et al.* [2006a,b] directly derived a formula for calculating RF_{T_1} using a single period approximation. Subsequently, Tsang *et al.* [2017] replaced this calculation formula of RF_{T_1} with a calculation chart. Miura *et al.* [2001] proposed formulae for calculating SAFRS at the first and second site fundamental periods based on one-dimensional wave theory. The response and limit strength calculation design method in the Japanese seismic code [Midorikawa *et al.*, 2003] incorporated Miura's approach to evaluate SAFRS at various periods. However, previous studies [Hayashi *et al.*, 2003; Koyamada *et al.*, 2004; Inoue *et al.*, 2010] have indicated that this method underestimates SAFRS when applied to multilayered soils and tends to overestimate SAFRS in the short period range. Moreover, evaluating nonlinear site effects using this approach requires complex iterative calculations. To address these challenges, Hayashi *et al.* [2003] developed formulae for calculating SAFRS at the first and second site fundamental periods without iterative calculations. However, these formulae are not applicable to actual multilayered soils. Koyamada *et al.* [2004] proposed a method for calculating RF_{T_1} in multilayered soils. Although this method can partially mitigate the underestimation issue of RF_{T_1} , the results remain highly unstable and can fluctuate significantly with changes in soil stratification. Inoue *et al.* [2010] proposed a method to evaluate nonlinear site effects on SAFRS using the response spectrum method within the response and limit strength calculation design method in the Japanese seismic code. Although this method improves accuracy, it still requires complex iterative calculations. To overcome these issues, Zhang *et al.* [2017a,b] and Zhang and Zhao [2018a,b, 2019] proposed a method that replaces the complex, multilayered site soils with a single-layer soil model, allowing for the accurate and efficient evaluation of the site fundamental period, T_1 , and RF_{T_1} . Subsequently, Zhang and Zhao [2021a] proposed a SAFRS model for various periods based on RF_{T_1} . However, all the aforementioned methods for evaluating SAFRS generally require site information, such as soil layer thickness and shear wave

velocity. Obtaining this information typically necessitates drilling, which is both complex to operate and costly to implement.

In this study, to avoid the use of such site information, a method is proposed to evaluate SAFRS using the microtremor horizontal-to-vertical spectral ratio (MHVSR). For this purpose, in Sec. 2, a formula for calculating RF_{T_1} using MHVSR is developed by analyzing microtremor data and site response results from 42 sites in Yokohama, Japan. To account for nonlinear site effects on SAFRS, Sec. 3 proposes formulae to estimate the rate of change of T_1 and RF_{T_1} under different ground motion intensities. In Sec. 4, by combining a SAFRS model developed for various periods from previous research, SAFRS at various periods are calculated based on T_1 and RF_{T_1} . Sec. 5 summarizes the procedures of the proposed method. In Sec. 6, the proposed method is validated and discussed based on linear and nonlinear site response analyses of 42 sites in Japan. Finally, the conclusions are presented in Sec. 7.

2. Expression for the SAFRS at the Site Fundamental Period

MHVSR has attracted widespread attention from scholars due to its low cost and simplicity of operation. This method was first proposed by Nakamura [1989] to estimate T_1 . Over the following decades, its application range has continuously expanded. MHVSR has been widely used in various fields, including sediment layer thickness estimation [Pranata *et al.*, 2018; Meng *et al.*, 2023], site classification [Laouami, 2020; Moustafa *et al.*, 2021], velocity structure inversion [Rong *et al.*, 2016; Maringue *et al.*, 2021; Manakou *et al.*, 2023; Aydin and Karimi, 2024; Combey *et al.*, 2024], and mineral exploration [Abu Zeid *et al.*, 2017; Yuliyanto and Harmoko, 2019; Cantwell *et al.*, 2019]. Currently, scholars have reached a consensus that MHVSR can reliably estimate T_1 [Sreejaya and Raghukanth, 2022]. Additionally, Nakamura [1989, 1996, 2000] pointed out that MHVSR at the site fundamental period, $MHVSR_{T_1}$, can characterize site amplification effects. Similarly, Akkaya *et al.* [2015] indicated that $MHVSR_{T_1}$ has a good correlation with site amplification effects. Therefore, this study proposes a method for evaluating SAFRS using MHVSR. First, this section develops a formula for calculating RF_{T_1} using MHVSR.

2.1. Microtremor data

To propose a method for evaluating SAFRS using MHVSR, this section selected 42 sites from the General Affairs Bureau of Yokohama City [GABYC, 2019], Japan, and obtained the corresponding borehole data. The geological map of the study area is shown in Fig. 1. The locations of the 42 sites are marked with black dots based on their corresponding latitude and longitude coordinates. The geological types, represented by different colors in Fig. 1, are explained in Table 1.

For each site, microtremor observations were conducted, and three components were recorded: two horizontal components (EW and NS) and one vertical component (UD). The sampling frequency was 100 Hz, and the observation time was 180 s.

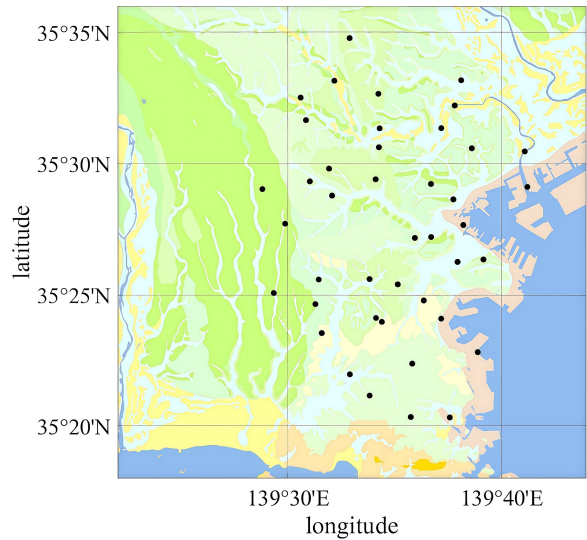


Fig. 1. Geological map of the study area.

Table 1. The geological types, represented by different colors in Fig. 1.







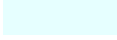

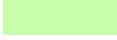
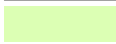
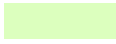
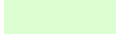
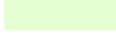
Color	Formative era	Rock and lithofacies
	Quaternary Holocene	Mature soil, buried land, and cultivated land
	Late Miocene Langian-Totonian	Marine stratified clastic rock
	Neogene Miocene-Messinian-Creocene	Marine stratified clastic rock
	Neogene Miocene-Messinian-Creocene	Andesite, basaltic andesite, trachyandesite, pyroclastic rock, pyroclastic rock, intrusive rock
	Quaternary Holocene	Coastal areas, sand dunes, and natural levee deposits
	Quaternary Pleistocene Diasian to Early Chivanian	Soda-layered mixed layer of seaweed and non-seaweed
	Quaternary Holocene	Valley plains, mountain basins, rivers, coastal plains, lakes, wetlands, and wetland deposits
	Late Quaternary Early Pleistocene	Duanqiu deposits
	Late Pleistocene Middle to Late Pleistocene	Duanqiu deposits

Table 1. (Continued)

Color	Formative era	Rock and lithofacies
	Quaternary Pleistocene Chivanian	Soda-layered mixed layer of seaweed and non-seaweed
	Quaternary Pleistocene Chivanian	Non-marine stratified clastic rock
	Late Pleistocene	Soda-layered mixed layer of seaweed and non-seaweed
	Quaternary Pleistocene Diasian to Early Chivanian	Marine stratified clastic rock

Although a longer observation time may yield better results [Havenith, 2004], the observation time was limited to 180 s due to time and site constraints. The impact of observation time on the research findings warrants further investigation in future studies. In addition, location information (latitude and longitude) and observation conditions were recorded using both maps and GPS. MHVSR was used to analyze the microtremor data. For each component (NS, EW, UD), segments of 20.48 s [Shi *et al.*, 2022b; Maringue *et al.*, 2021] with relatively stable signals were extracted from the observed waveform data. The Fourier amplitude spectrum was then calculated for each segment and smoothed using a Parzen window with a bandwidth of 0.3 Hz. The geometric mean of the Fourier amplitude spectrum of the two horizontal components was calculated for each segment, and then divided by the vertical component to obtain the MHVSR curve. Finally, the MHVSR curves of all the extracted intervals were averaged [Ochiai *et al.*, 2019].

By analyzing the microtremor data, it was found that the MHVSR curves exhibit various patterns, including single peaks, double peaks, multiple peaks, and cases with no clear peaks. For single peaks, the horizontal coordinate corresponding to the peak is directly extracted as T_1 , and the vertical coordinate corresponding to T_1 is $MHVSR_{T_1}$. For double peaks and multiple peaks, considering the shallow foundation of Yokohama City [Ochiai *et al.*, 2019], the horizontal coordinate corresponding to the short-period peak is designated as T_1 , and the vertical coordinate corresponding to T_1 is denoted as $MHVSR_{T_1}$. For sites with no obvious peaks, it is assumed that the site is hard and that site amplification effects are not significant. The T_1 and corresponding $MHVSR_{T_1}$ values obtained from the microtremor data of the 42 sites are shown in Table 2.

Because this study primarily focuses on shallow surface soil, MHVSR with periods ranging from 0.1 s to 2.0 s is considered. In addition, if $MHVSR_{T_1}$ is less than 2.0, the site is considered relatively hard, with negligible site amplification effects [Wen *et al.*, 2015]. From Table 2, it can be seen that sites No. 10, No. 11, No. 12, No. 19, No. 20, No. 21, No. 22, No. 32, No. 33, No. 38, No. 39, No. 40, and No. 41 are hard. Therefore,

Table 2. T_1 and $MHVS_{R_{T_1}}$ values for the 42 sites considered in this study.

Site	T_1	$MHVS_{R_{T_1}}$	Site	T_1	$MHVS_{R_{T_1}}$
No. 01	0.293	2.850	No. 22	0.256	1.085
No. 02	0.372	2.080	No. 23	0.269	2.388
No. 03	0.310	2.570	No. 24	0.427	2.244
No. 04	0.465	2.827	No. 25	0.853	3.258
No. 05	0.394	2.650	No. 26	0.336	3.610
No. 06	0.585	4.142	No. 27	0.436	2.515
No. 07	1.463	3.977	No. 28	0.301	2.758
No. 08	1.205	2.993	No. 29	0.731	2.078
No. 09	0.621	3.039	No. 30	0.188	2.206
No. 10	0.139	1.818	No. 31	0.273	4.852
No. 11	0.64	1.621	No. 32	0.759	1.874
No. 12	0.683	1.278	No. 33	0.585	1.985
No. 13	0.325	2.367	No. 34	0.359	2.259
No. 14	0.205	2.820	No. 35	0.621	2.564
No. 15	0.401	2.749	No. 36	0.259	2.313
No. 16	0.233	3.523	No. 37	0.233	2.997
No. 17	0.106	2.717	No. 38	0.269	1.713
No. 18	0.253	2.54	No. 39	0.269	1.959
No. 19	0.306	1.551	No. 40	0.205	1.035
No. 20	0.147	1.492	No. 41	0.269	1.346
No. 21	0.193	1.431	No. 42	0.353	2.746

this study focuses on the remaining 29 sites. In addition, the shear wave velocity profiles of these 29 sites, obtained from the General Affairs Bureau of Yokohama City [GABYC, 2019], are presented in Fig. 2. The figure shows the variation in shear wave velocity at different depths, characterizing the soil structure at each site. The x -axis represents the shear wave velocity (m/s), while the y -axis represents depth (m).

2.2. Expression for the SAFRS at the site fundamental period

To derive the formula for evaluating RF_{T_1} using $MHVS_{R_{T_1}}$, linear site response analyses are performed for the 29 sites in Sec. 2.1 using the SHAKE program [Schnabel, 1972]. The damping ratio of soil and bedrock are set as 2.5% and 0, respectively, based on the study by Bard and Bouchon [1985]. The damping ratio of bedrock is set to 0 due to its high stiffness and low energy dissipation characteristics. The shear wave velocity and layer thickness for each site are taken from Fig. 2, while the density data are sourced from the General Affairs Bureau of Yokohama City [GABYC, 2019]. Subsequently, the transfer functions for each site are obtained, and accordingly, T_1 and RF_{T_1} are extracted. The T_1 results obtained using the SHAKE program are compared with those obtained by $MHVS_{R_{T_1}}$ in Fig. 3(a). In addition, the RF_{T_1} results obtained using the SHAKE program are compared with those from $MHVS_{R_{T_1}}$ in Fig. 3(b). From Fig. 3(a), it can be observed that the T_1 results from both methods are essentially consistent, validating the effectiveness of $MHVS_{R_{T_1}}$ in evaluating T_1 . However, in Fig. 3(b), the RF_{T_1} results obtained using the SHAKE

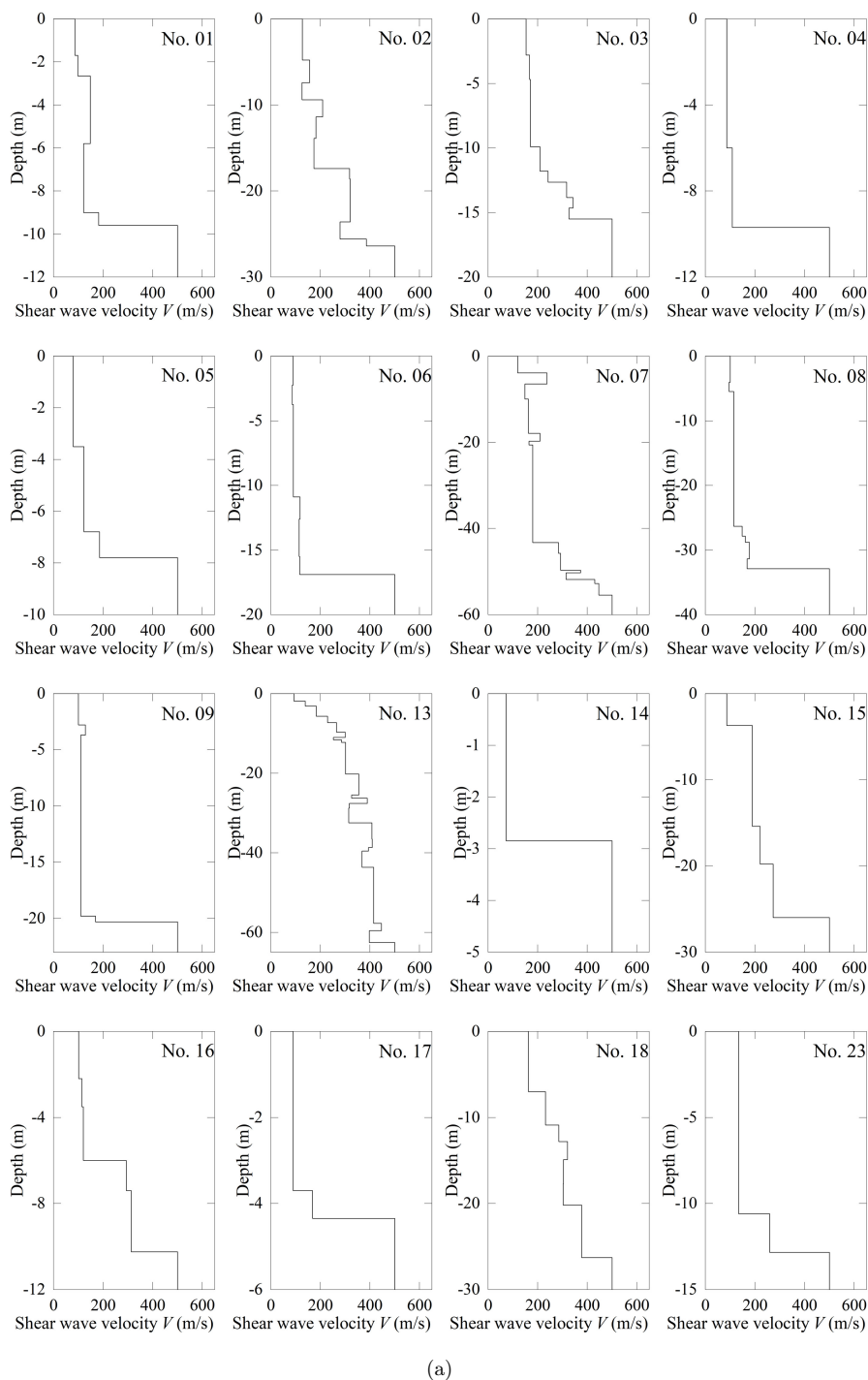
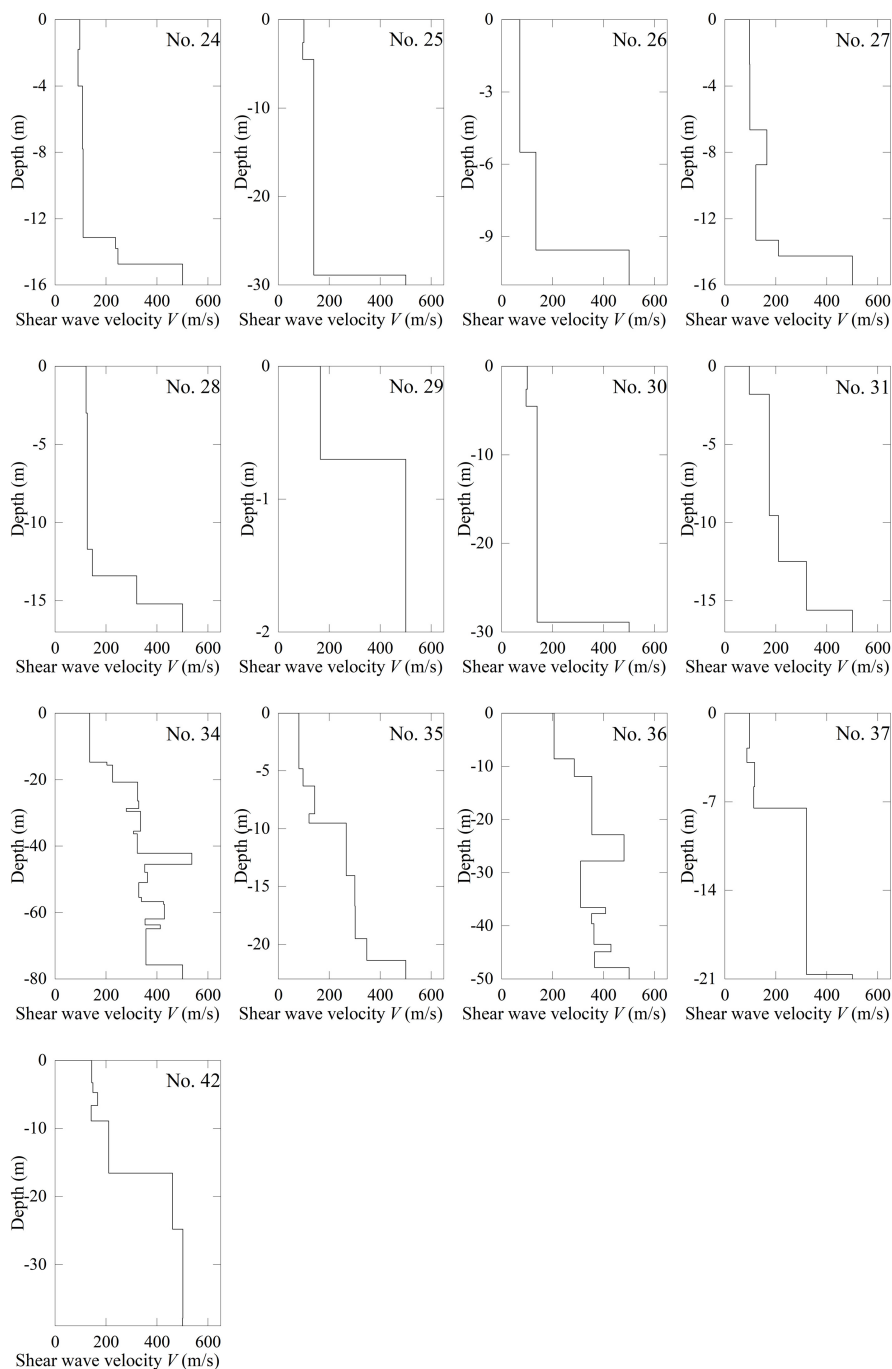


Fig. 2. Shear wave velocity profiles for 29 sites.



(b)

Fig. 2. (Continued)

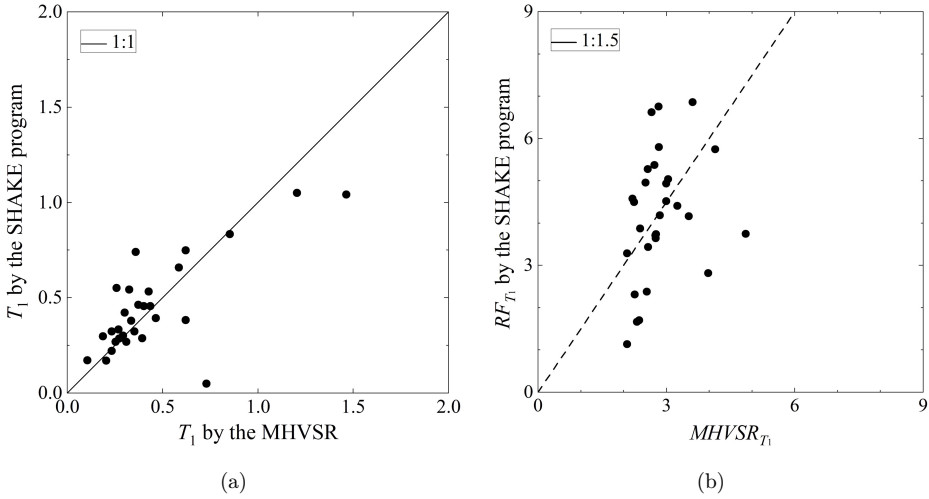


Fig. 3. Comparison of results obtained by MHVSR with those obtained from the SHAKE program in 29 sites.

program and MHVSR show a significant difference. Then, a formula for evaluating RF_{T_1} from $MHVSR_{T_1}$ is then regressed as

$$RF_{T_1} = 1.5MHVSR_{T_1}. \quad (1)$$

Equation (1) is derived through linear regression analysis based on the least squares method. Furthermore, the regression coefficients are simplified, retaining only one decimal place, set to 1.5. Although the mean absolute error is 1.1928, the trend between RF_{T_1} and $MHVSR_{T_1}$ is consistent with the trend predicted by the regression formula. To simplify the fitting expression, some compromises are made in terms of accuracy. By applying Eq. (1), RF_{T_1} can be obtained based on the MHVSR.

3. Effects of Site Nonlinearity

In Sec. 2, T_1 and RF_{T_1} , obtained using MHVSR, are considered in the linear state, where the soil is assumed to behave as a linear material. However, when considering design earthquakes, in which the seismic input is sufficiently large to induce significant soil strain, the soil exhibits nonlinear behavior [Beresnev and Wen, 1996]. This nonlinear behavior, in turn, affects T_1 and RF_{T_1} . Therefore, when proposing a method for evaluating SAFRS for seismic design, it is essential to account for the influence of nonlinearity.

To assess the effects of site nonlinearity on T_1 and RF_{T_1} , ten moderate-intensity and ten high-intensity ground motions are generated using View Wave [2019], based on the bedrock response spectra corresponding to moderate- and high-intensity ground motions as defined in the response and limit strength calculation design method in the Japanese seismic code [Midorikawa et al., 2003; BHMI, 2001, 2007].

The peak ground accelerations of the moderate- and high-intensity ground motions are 64 cm/s^2 and 320 cm/s^2 , respectively. Subsequently, T_1 and RF_{T_1} are calculated for each site for moderate- and high-intensity ground motions considering both linear and nonlinear soil behaviors using the SHAKE program [Schnabel, 1972].

Based on the above results, an equation for the ratio of T_1 under moderate-intensity ground motions, considering soil nonlinearity, T_{NM} , to T_1 in the linear state, T_L , is regressed as

$$T_{NM}/T_L = 0.95 + 0.19T_L + 0.02RF_{T_L}, \quad (2)$$

where RF_{T_L} represents RF_{T_1} in the linear state. Similarly, an equation for the ratio of RF_{T_1} under moderate-intensity ground motions, considering soil nonlinearity, $RF_{T_{NM}}$, to RF_{T_L} , is derived as

$$RF_{T_{NM}}/RF_{T_L} = 1.106 - 0.02RF_{T_L}. \quad (3)$$

In addition, an equation for T_1 under high-intensity ground motions, T_{NH} , to T_L is regressed as

$$T_{NH}/T_L = 0.34 + 0.68T_L + 0.33RF_{T_L}. \quad (4)$$

Similarly, an equation for the ratio of the RF_{T_1} under high-intensity ground motions, $RF_{T_{NH}}$, to RF_{T_L} is regressed as

$$RF_{T_{NH}}/RF_{T_L} = 1.22 - 0.02T_L - 0.1RF_{T_L}. \quad (5)$$

Then, based on Eqs. (2)–(5), T_1 and RF_{T_1} under moderate- and high-intensity ground motions can be obtained. To verify the accuracy of the regression analysis, the results obtained from Eqs. (2)–(5) are compared with those obtained using the SHAKE program under moderate- and high-intensity ground motions. The results are shown in Figs. 4(a) and 4(b). Figure 4(a) presents the results of T_{NM}/T_L and T_{NH}/T_L , while Fig. 4(b) presents the results of $RF_{T_{NM}}/RF_{T_L}$ and $RF_{T_{NH}}/RF_{T_L}$. For T_{NM}/T_L results, the average relative error is only 4.3%, with a maximum relative error of 11.17%. For T_{NH}/T_L results, the average relative error is 12.5%, and 82.7% of the results have a relative error within 20%. For $RF_{T_{NM}}/RF_{T_L}$ results, the average relative error is only 2.9%, with a maximum relative error of 9.76%. For $RF_{T_{NH}}/RF_{T_L}$ results, the average relative error is 8.0%, and 96.5% of the results have a relative error within 20%.

4. Expression for Site Amplification Factor of Response Spectrum

In Secs. 2 and 3, T_1 and RF_{T_1} are obtained for moderate- and high-intensity ground motions, considering both linear and nonlinear soil behaviors. However, SAFRS is a function of period. To calculate SAFRS at various periods based on T_1 and RF_{T_1} , it is necessary to combine a full-period evaluation model. After reviewing existing SAFRS models, the model proposed by Zhang and Zhao [2021a] was ultimately adopted. This model is based on random vibration theory and wave propagation theory,

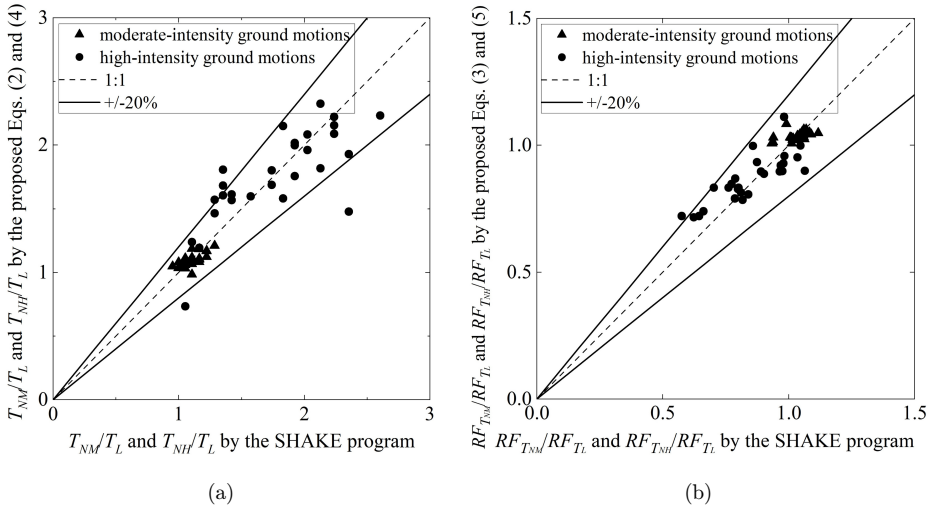


Fig. 4. Comparisons of the results obtained by the proposed formulae with those obtained by the SHAKE program under moderate- and high-intensity ground motions, considering soil nonlinearity.

incorporating seismic scenario effects. The model is developed using the site transfer function of a single-layer soil model, which is expressed as follows:

$$RSR(T_0) = \begin{cases} (RF_{T_1} - RPA) \left[\left(\frac{T_0}{T_1} \right)^{1.5} - 1 \right] + RF_{T_1} & T_0 \leq T_1, \\ RF_{T_1} & T_1 < T_0 \leq 1.1T_1, \\ (RF_{T_1} - 1) \left[\left(\frac{1.1T_1}{T_0} \right)^{1.5} - 1 \right] + RF_{T_1} & 1.1T_1 < T_0, \end{cases} \quad (6)$$

where RSR corresponds to the SAFRS in this study, T_0 is the oscillator period or the natural period of the single degree of freedom system, and RPA is the site amplification ratio for the peak acceleration. The SAFRS model is controlled by three key parameters, viz. T_1 , RF_{T_1} and RPA . Among these, T_1 and RF_{T_1} can be obtained by the proposed equations based on MHVSR in Secs. 2 and 3. RPA can be obtained using the following equation [Zhang and Zhao, 2021a]:

$$RPA = \frac{2}{1+a} \exp \left(-\frac{\pi}{2} \frac{T_1}{T_F} h \right), \quad (7)$$

where a is the impedance ratio of the soil layer to the rock layer, which can be obtained using the following equation [Zhang and Zhao, 2018a]:

$$a = \frac{1}{RF_{T_1}} - 1.57h, \quad (8)$$

where h is the soil damping ratio. In this study, the value of h is assumed to be 2.5%. Although h may increase to some extent in the nonlinear soil state, it does not affect the results of this study.

In Eq. (7), T_F represents the period at which the site transfer function equals RPA . The formula is as follows:

$$T_F = 1.5T_P, \quad (9)$$

where T_P corresponds to the mean value of the first and second corner periods, which mark the start and end of the acceleration plateau in the bedrock spectrum. Based on these equations, SAFRS at various periods can be evaluated using MHVSR.

Notably, the full-period SAFRS model proposed by Zhang and Zhao [2021a] and adopted in this study considers only a single peak and assumes linearity for short periods despite the potential presence of multiple peaks in SAFRS. This simplification is primarily intended to meet the practical requirements of engineering applications, as accounting for multiple peaks would introduce additional complexity. Moreover, the largest peak, which is the primary focus of this study, can be easily identified using MHVSR, whereas smaller secondary peaks may be more challenging to distinguish. Additionally, since the largest peak generally dominates the site response, the influence of other peaks on the overall results is relatively minimal, particularly for the shallow soil profiles relevant to engineering practice.

5. Procedure of the Proposed Method

In conclusion, the procedure of the proposed method can be summarized in the following steps, as shown in Fig. 5.

Step 1: Conduct microtremor observations at the site of interest to obtain the microtremor data.

Step 2: Calculate the MHVSR curve using the microtremor data.

Step 3: Extract the site fundamental period T_1 and the corresponding peak $MHVSR_{T_1}$ from the MHVSR curve. For MHVSR curves with a single peak, T_1 and $MHVSR_{T_1}$ are determined based on this peak. For curves with multiple peaks, T_1 and $MHVSR_{T_1}$ are derived from the peak corresponding to the shorter period. If the MHVSR curve shows no distinct peaks or if the peak value is less than 2, the site is considered to have no significant amplification effect, and no further calculations are required.

Step 4: Calculate the site fundamental period T_L and the corresponding peak RF_{T_L} for SAFRS in the linear state using Eq. (1), based on T_1 and $MHVSR_{T_1}$ obtained in Step 3.

Step 5: Calculate the site fundamental periods and corresponding peaks under moderate- and high-intensity ground motions, considering soil nonlinearity, i.e., T_{NM} and $RF_{T_{NM}}$ as well as T_{NH} and $RF_{T_{NH}}$, using Eqs. (2) and (3) and Eqs. (4) and (5), respectively, based on T_L and RF_{T_L} obtained in Step 4.

Step 6: Calculate SAFRS at various periods using Eq. (6) based on the site fundamental periods and corresponding peaks from Step 5.

To further clarify the calculation procedure of the proposed method, an example calculation using site No. 27 is presented. First, the MHVSR curve is derived from

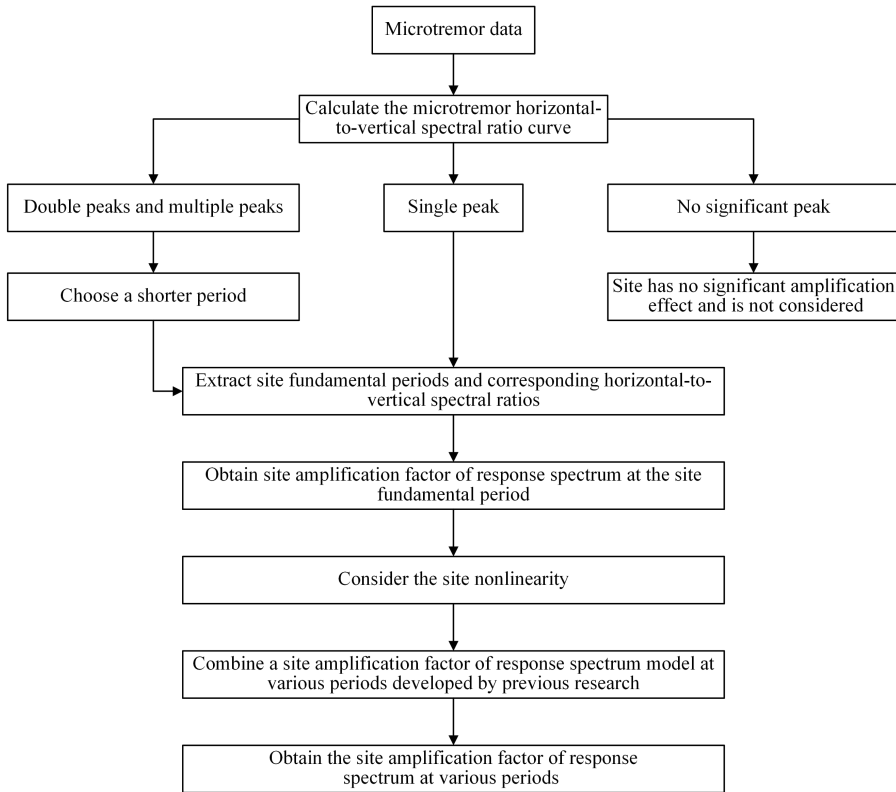


Fig. 5. Flowchart for evaluating SAFRS using MHVSR.

microtremor data, as depicted by the black curve in Fig. 6. Based on this curve, the site fundamental period T_1 is determined to be 0.436 s, with the corresponding peak $MHVSR_{T_1}$ of 2.515, as shown in Table 3. Next, using Eq. (1), the site fundamental period T_L and the corresponding peak RF_{T_L} for SAFRS in the linear state are

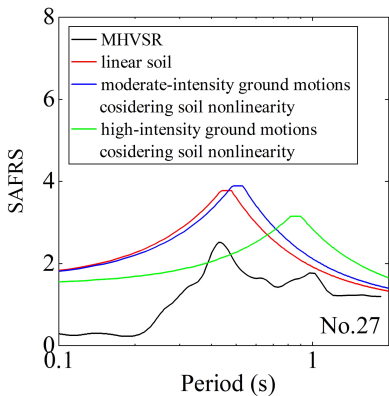


Fig. 6. SAFRS of site No. 27 calculated using the proposed method.

Table 3. The step-by-step results of applying the proposed method to site No. 27.

Calculation item		Parameter	Result
	MHVSR curve	T_1	0.43600
		$MHVSR_{T_1}$	2.51500
	Linear soil	T_L	0.43600
		RF_{T_L}	3.77250
Nonlinear soil	Moderate-intensity ground motions	T_{NM}	0.48321
		$RF_{T_{NM}}$	3.88775
	High-intensity ground motions	T_{NH}	0.82029
		$RF_{T_{NH}}$	3.14638

obtained as 0.436 s and 3.7725, respectively. Considering soil nonlinearity, the site fundamental period T_{NM} and the corresponding peak $RF_{T_{NM}}$ for SAFRS under moderate-intensity ground motions are determined using Eqs. (2) and (3), with the values of 0.48321 s and 3.88775, respectively. Similarly, for high-intensity ground motions, the site fundamental period T_{NH} and the corresponding peak $RF_{T_{NH}}$ are obtained using Eqs. (4) and (5), with the values of 0.82029 s and 3.14638, respectively. Finally, SAFRS at various periods, accounting for moderate- and high-intensity ground motions and considering both linear and nonlinear soil behaviors, are evaluated, with the results illustrated in Fig. 6.

6. Verification and Discussion

6.1. Verification of the proposed method for the linear state

To validate the accuracy of the proposed method in the linear state, SAFRS for each site are calculated using the SHAKE program under the assumption that the soil behaves as a linear material. The results are then compared with those obtained from the proposed method and are presented in Fig. 7. From Fig. 7, it can be seen that for sites No. 01, No. 02, No. 04, No. 06, No. 08, No. 09, No. 13, No. 15, No. 23, No. 24, No. 25, No. 26, No. 27, No. 30, No. 34, No. 35, and No. 37, the peak values of SAFRS obtained by the proposed method are generally consistent with those from the SHAKE program. This indicates that the proposed method performs well. For sites No. 03, No. 07, No. 16, No. 18, No. 28, No. 29, and No. 42, the peak values of SAFRS obtained by the proposed method are higher than those of the SHAKE program, indicating that the calculation results are somewhat conservative. For sites No. 05, No. 14, No. 17, No. 31, and No. 36, the peak values of SAFRS obtained by the proposed method are slightly lower than those from the SHAKE program, but the deviation is not significant. To quantify the difference between the SAFRS obtained by the proposed method and that from the SHAKE program, the ratio of the peak value of SAFRS from the proposed method to the average peak value of SAFRS from the SHAKE program, denoted as R_P , is calculated. The R_P values for each site are presented in Fig. 7. As observed, 69% of the sites have R_P values ranging from 0.7 to 1.3. In general, the SAFRS results obtained by the proposed method demonstrate

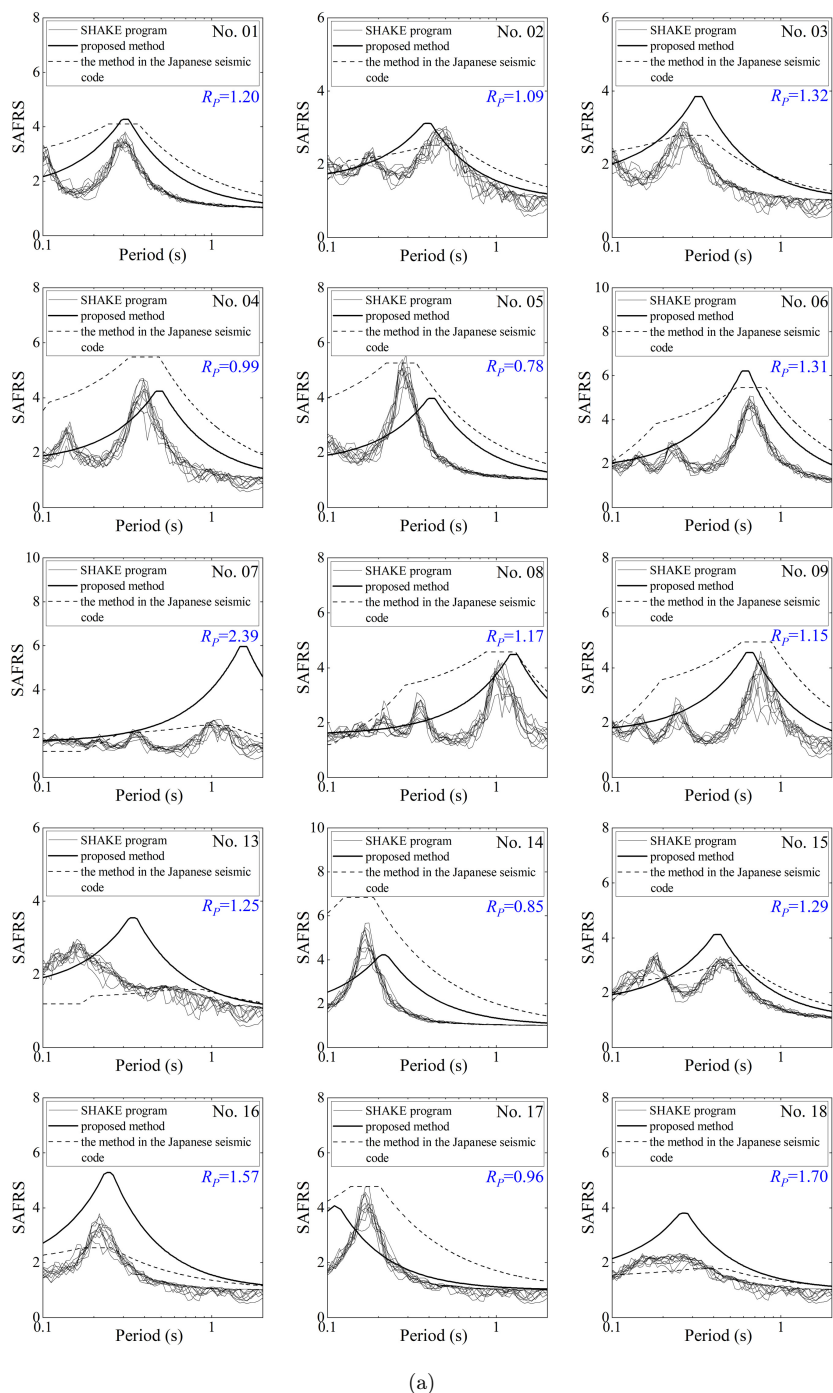


Fig. 7. Comparison of the SAFRS calculated by the SHAKE program, the proposed method, and the method in the Japanese seismic code under the linear state.

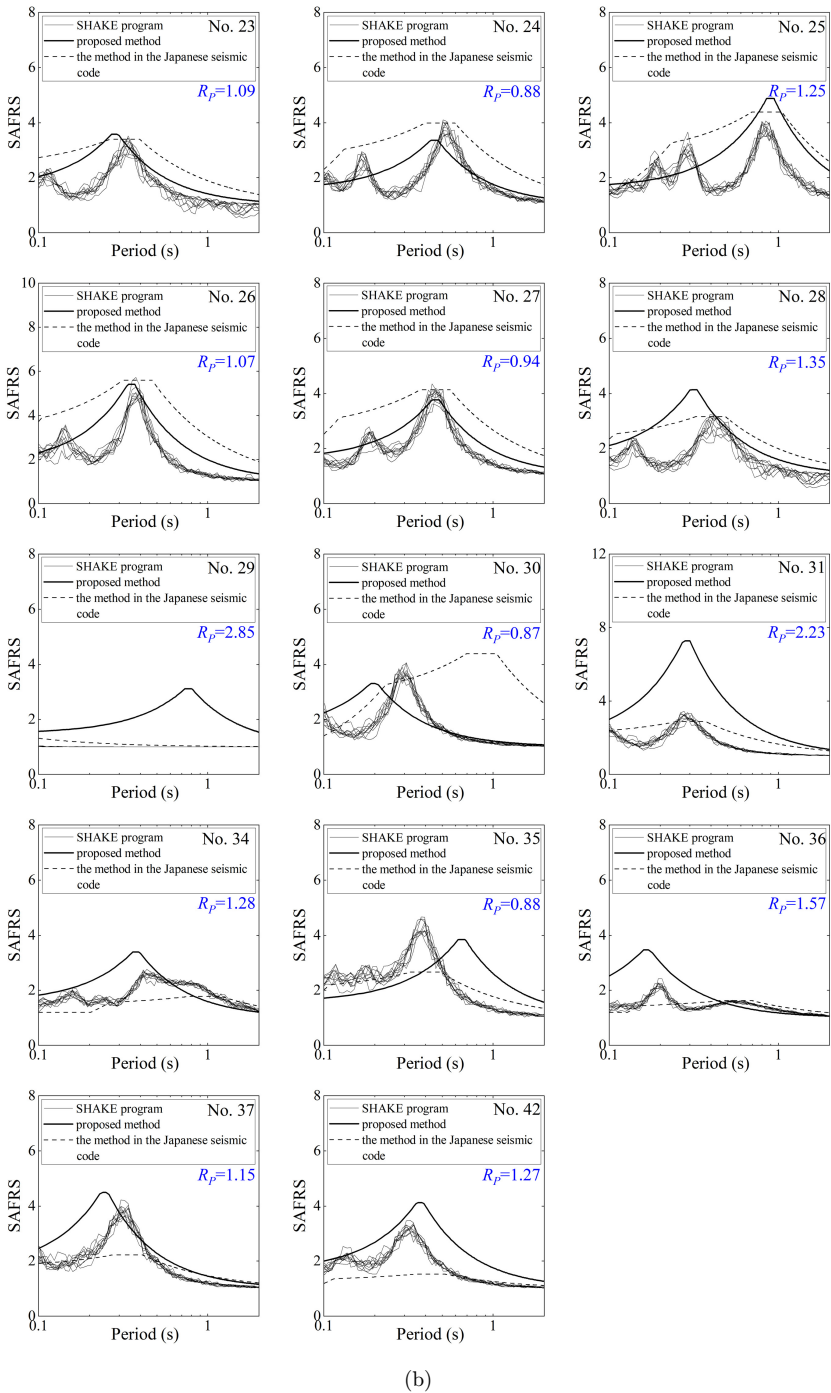


Fig. 7. (Continued)

good performance, thereby validating the accuracy of the proposed method for evaluating SAFRS in the linear state.

In addition, as shown in Fig. 7, a significant discrepancy is observed between SAFRS obtained using the proposed method and those derived from the SHAKE program at certain sites, such as sites No. 07, No. 18, No. 29, and No. 31. This discrepancy is primarily attributed to two factors. First, there is an inconsistency in the soil depth considered in site response analyses and MHVSR. The borehole data available for site response analyses is limited to shallow depths, whereas microtremor data may capture deeper geological effects. For instance, at site No. 29, the available soil data extends to only 0.7 m, leading to significant discrepancies in T_1 , which are also evident in Fig. 3(a). Second, the application of Eq. (1) for estimating RF_{T_1} introduces considerable errors in certain cases, as discussed in detail in Sec. 2.2 (Fig. 3(b)). These errors result in discrepancies in the amplitudes of SAFRS, such as site No. 07, No. 18, and No. 31.

Moreover, the SAFRS under the linear state is calculated using the response and limit strength calculation design method in the Japanese seismic code, with the results presented in Fig. 7. As shown in Fig. 7, the SAFRS calculated using the method in the Japanese seismic code, particularly the peak values, are slightly closer to those obtained from the SHAKE program compared to the proposed method. This is because both the method in the Japanese seismic code and the SHAKE program are based on one-dimensional wave propagation theory, with the former essentially serving as an approximation of the latter.

6.2. Verification of the proposed method for the nonlinear state

To verify the accuracy of the proposed method under moderate-intensity ground motions, considering soil nonlinearity, the SAFRS are calculated for each site using the SHAKE program based on the ten moderate-intensity ground motions generated in Sec. 3. The results are then compared with those obtained from the proposed method and are presented in Fig. 8. From Fig. 8, it can be seen that for sites No. 01, No. 02, No. 03, No. 04, No. 08, No. 09, No. 13, No. 14, No. 15, No. 23, No. 24, No. 26, No. 27, No. 34, No. 37, and No. 42, the peak values of SAFRS obtained by the proposed method are generally consistent with those obtained by the SHAKE program. This indicates that the proposed method performs well. For sites No. 06, No. 07, No. 16, No. 18, No. 25, No. 28, No. 29, No. 31, and No. 36, the peak values of SAFRS obtained by the proposed method are higher than those obtained by the SHAKE program, indicating that the calculation results are conservative. For sites No. 05, No. 17, No. 30, and No. 35, the peak values of SAFRS obtained by the proposed method are slightly lower than those obtained by the SHAKE program, but the deviation is not significant. To quantify the difference between the SAFRS obtained by the proposed method and the SHAKE program, the R_p values for each site are presented in Fig. 8. As observed, 76% of the sites have R_p values ranging from 0.7 to 1.3. In general, the SAFRS results obtained by the proposed method show

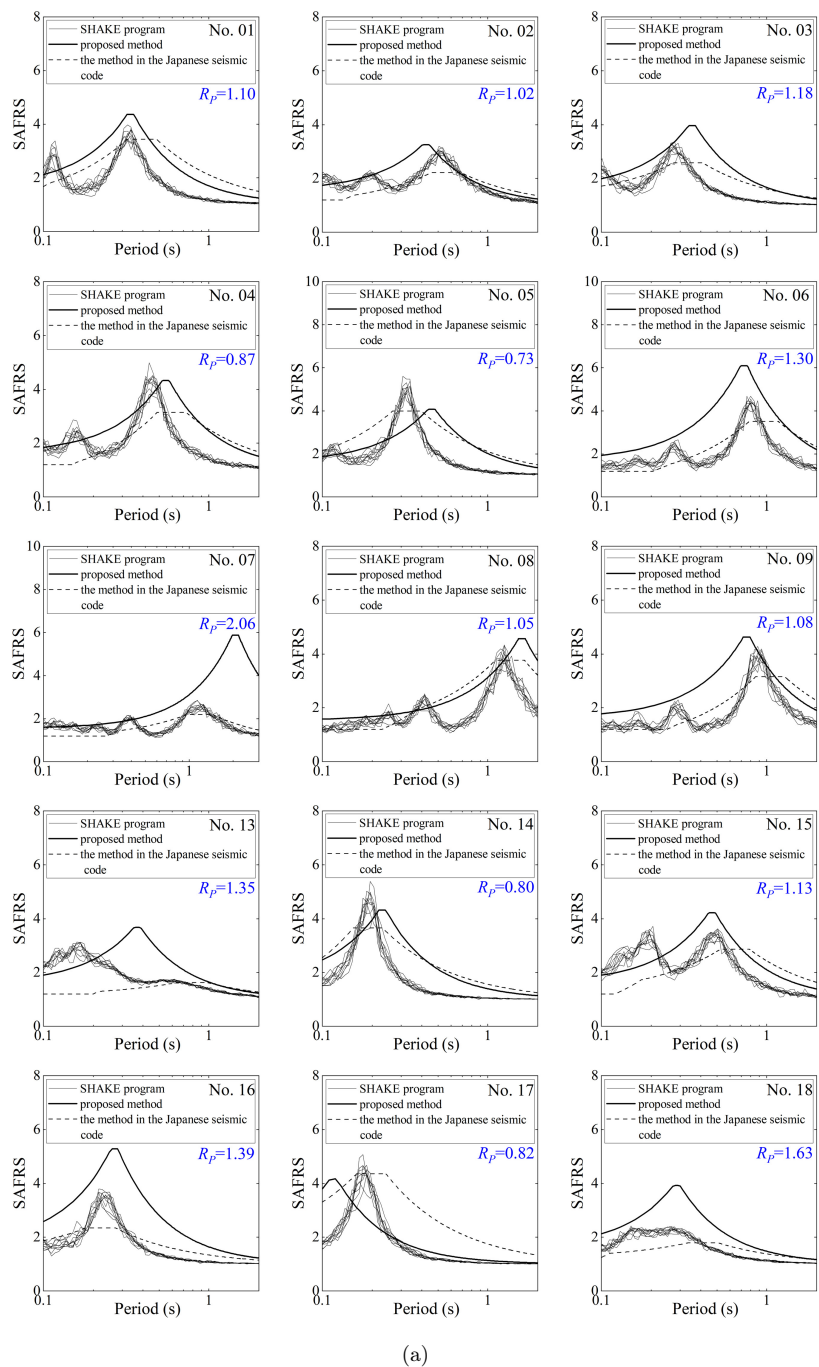


Fig. 8. Comparison of the SAFRS calculated by the SHAKE program, the proposed method, and the method in the Japanese seismic code under moderate-intensity ground motions, considering soil nonlinearity.

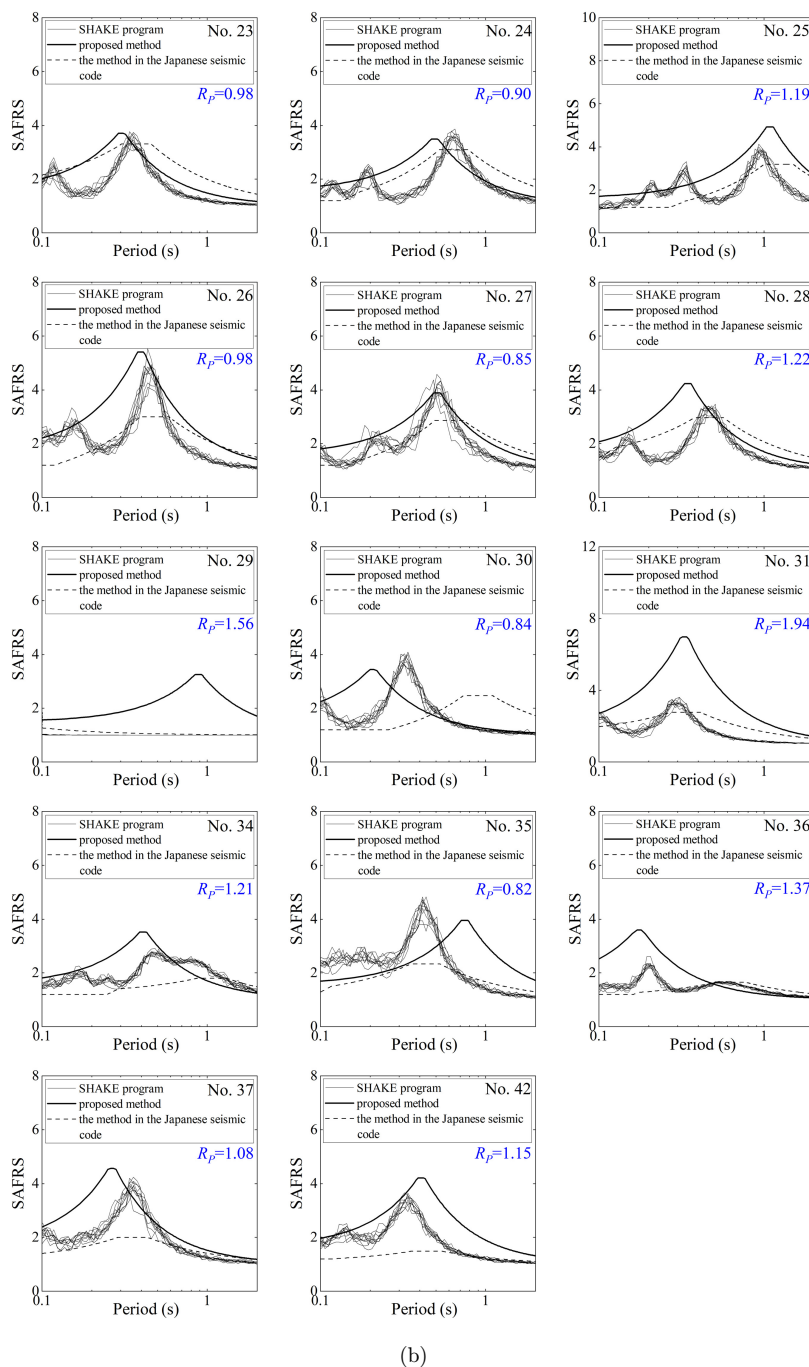


Fig. 8. (Continued)

good performance, thereby validating the accuracy of the proposed method in evaluating SAFRS under moderate-intensity ground motions, considering soil nonlinearity.

In addition, the SAFRS under moderate-intensity ground motions is calculated using the response and limit strength calculation design method in the Japanese seismic code, with the results presented in Fig. 8. As shown in Fig. 8, overall, the SAFRS calculated using the method in the Japanese seismic code is lower than those obtained by the SHAKE program, while the SAFRS calculated using the proposed method is slightly higher than those obtained by the SHAKE program.

To verify the accuracy of the proposed method under high-intensity ground motions, considering soil nonlinearity, the SAFRS are calculated for each site using the SHAKE program based on the 10 high-intensity ground motions generated in Sec. 3. The results are then compared with those obtained from the proposed method and are presented in Fig. 9. From Fig. 9, it can be seen that for sites No. 01, No. 02, No. 03, No. 04, No. 08, No. 09, No. 13, No. 14, No. 15, No. 17, No. 23, No. 24, No. 26, No. 27, No. 30, No. 34, and No. 37, the peak values of SAFRS obtained by the proposed method are generally consistent with those by the SHAKE program. This indicates that the proposed method performs well. For sites No. 06, No. 07, No. 16, No. 18, No. 25, No. 28, No. 29, No. 31, No. 36, and No. 42, the peak values of SAFRS obtained by the proposed method are higher than those obtained by the SHAKE program, indicating that the calculated results are conservative. For sites No. 05 and No. 35, the peak values of SAFRS obtained by the proposed method are slightly lower than those obtained by the SHAKE program, but the deviation is not significant. To quantify the difference between the SAFRS obtained by the proposed method and the SHAKE program, the R_P values for each site are presented in Fig. 9. As observed, 90% of the sites have R_P values ranging from 0.7 to 1.3. In general, the SAFRS results obtained by the proposed method show good performance, thus validating the accuracy of the proposed method in evaluating SAFRS under high-intensity ground motions, considering soil nonlinearity.

In addition, the SAFRS under high-intensity ground motions is calculated using the response and limit strength calculation design method in the Japanese seismic code, with the results presented in Fig. 9. As shown in Fig. 9, overall, the SAFRS calculated using the method in the Japanese seismic code is lower than those obtained by the SHAKE program, while the SAFRS calculated using the proposed method, particularly the peak values, are generally consistent with those obtained by the SHAKE program.

In conclusion, the accuracy of the proposed method is comparable to that of the method in the Japanese seismic code when compared to the SHAKE program. However, similar to the SHAKE program, the method in the Japanese seismic code not only requires borehole data but also involves complex iterative calculations when accounting for soil nonlinearity. In contrast, the proposed method only requires microtremor data, eliminating the need for borehole data and complex iterative calculations, thus enabling a more efficient evaluation of SAFRS at various periods.

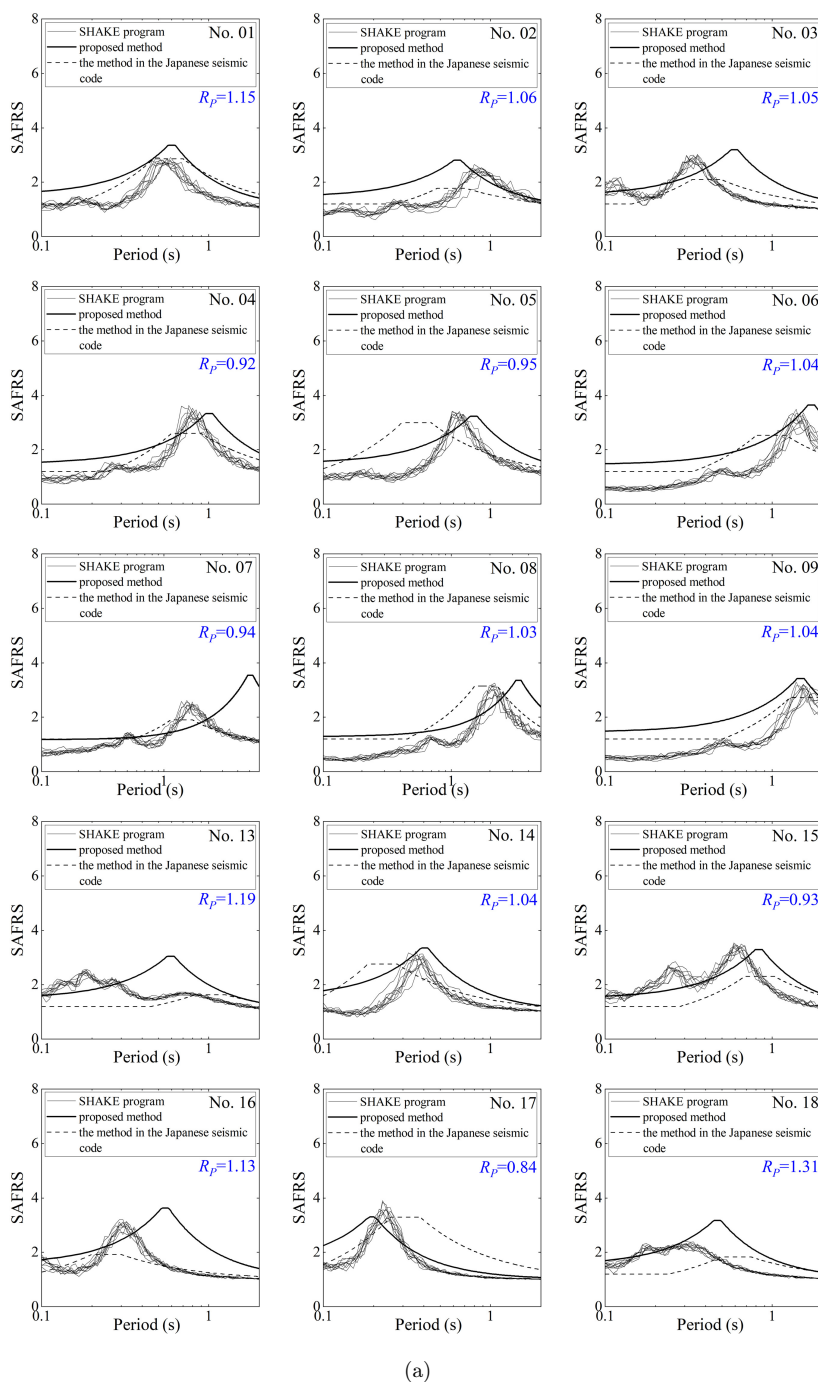


Fig. 9. Comparison of the SAFRS calculated by the SHAKE program, the proposed method, and the method in the Japanese seismic code under high-intensity ground motions considering soil nonlinearity.

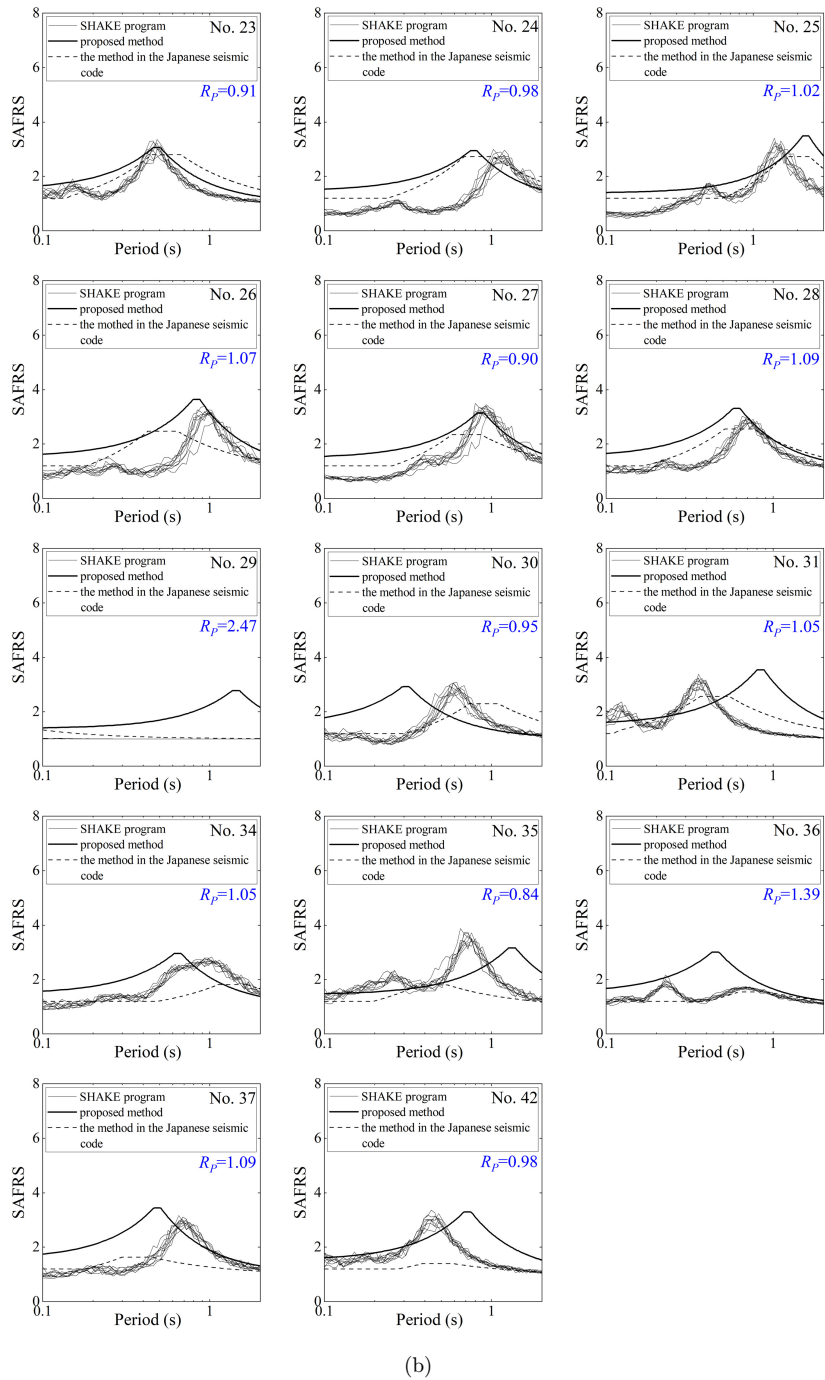


Fig. 9. (Continued)

7. Conclusions

This study proposes a method to evaluate SAFRS using the MHVSR, which requires no site-specific information, such as soil layer thickness and shear wave velocity. To this end, a formula is developed to calculate the SAFRS at the site fundamental period using MHVSR, based on microtremor data and site response analyses from 42 sites in Yokohama, Japan. Additionally, to account for nonlinear site effects on SAFRS, relationships are established to describe the variation in the site fundamental period, T_1 , and the corresponding SAFRS, RF_{T_1} , as a function of ground-motion intensity. Furthermore, by incorporating previously developed SAFRS models for various periods, a method for rapidly estimating SAFRS at various periods is proposed. Finally, the effectiveness of the proposed method is validated through linear and nonlinear site response analyses and compared with the response and limit strength calculation design method in the Japanese seismic code. The proposed method is simple, cost-effective, and expected to have significant engineering applications. The main conclusions of this study can be summarized as follows:

- (1) The effectiveness of using MHVSR to evaluate T_1 is validated by comparing results obtained from MHVSR with those derived from site response analyses.
- (2) The formulae developed for estimating site nonlinearity effects on T_1 and RF_{T_1} exhibit good consistency with the results from the SHAKE program under moderate- and high-intensity ground motions.
- (3) The SAFRS calculated by the proposed method generally agrees well with those obtained from the SHAKE program. In the linear state, the ratio of the peak value of SAFRS from the proposed method to the average peak value of SAFRS from the SHAKE program, R_p , falls within the range of 0.7–1.3 for 69% of sites. When accounting for soil nonlinearity, R_p remains within this range for 76% of sites under moderate-intensity ground motions and 90% of sites under high-intensity ground motions.
- (4) The proposed method and the method in the Japanese seismic code demonstrate similar accuracy in estimating SAFRS compared to the SHAKE program. However, unlike the SHAKE program and the method in the Japanese seismic code, which require borehole data and complex iterative calculations for nonlinearity, the proposed method relies only on microtremor data to effectively evaluate SAFRS at various periods.

Although the proposed method is useful in regions lacking borehole data for evaluating SAFRS, it is derived from data collected at 29 sites in Yokohama, Japan, and may, therefore, be most applicable to this specific region. Given the potential regional differences, it is essential to carefully consider, validate, or adjust the method when extending its application to other regions to ensure its accuracy and reliability.

Acknowledgments

This study was partially supported by the National Natural Science Foundation of China (Grant No. 52278135). The micromotion data used in this study were provided by Mr. Ochiai from Kanagawa University, Japan. The authors are grateful for this support.

References

- Abu Zeid, N., Corradini, E., Bignardi, S., Nizzo, V. and Santarato, G. [2017] "The passive seismic technique 'HVSr' as a reconnaissance tool for mapping paleo-soils: The case of the Pilastrì archaeological site, Northern Italy," *Archaeol. Prospect.* **24**(3), 245–258.
- Akkaya, I., Özvan, A., Tapan, M. and Şengül, M. A. [2015] "Determining the site effects of 23 October 2011 earthquake (Van province, Turkey) on the rural areas using HVSr microtremor method," *J. Earth Syst. Sci.* **124**, 1429–1443.
- ASCE/SEI 7-10 [2010] *Minimum Design Loads for Buildings and Other Structures* (American Society of Civil Engineers, America).
- Aydin, Ö. L. and Karimi, B. [2024] "Application of the MHVSr method for determining the location of landslide areas before geotechnical project proposal: A case study of Tortum Lake, Turkey," *Acta Geophys.* **72**(5), 3139–3158.
- Baoyintu and Kawase, H. [2021] "Quantitative evaluation of the seismic reinforcement effect based on observed microtremors," *J. Earthq. Tsunami* **15**(5), 2150021.
- Bard, P. Y. and Bouchon, M. [1985] "The two-dimensional resonance of sediment-filled valleys," *Bull. Seismol. Soc. Am.* **75**(2), 519–541.
- Beresnev, I. A. and Wen, K. L. [1996] "Nonlinear soil response — A reality?" *Bull. Seismol. Soc. Am.* **86**(6), 1964–1978.
- BHMI [2001] *Examples and Introduction of Calculation Method of Response and Limit Strength* (Building Instruction Department, Housing Administration, Ministry of Land, Infrastructure Transport and Tourism, Japan).
- BHMI [2007] *Structure-Related Technical Standard Commentary Book of the Building* (Building Instruction Department, Housing Administration, Ministry of Land, Infrastructure Transport and Tourism, Japan).
- Borcherdt, R. D. [1994] "Estimates of site-dependent response spectra for design (methodology and justification)," *Earthq. Spectra* **10**(4), 617–653.
- Bozdogan, K. B. and Keskin, E. [2024] "A method for determining the fundamental site period and the average shear wave velocity," *J. Earthq. Tsunami* **18**(5), 2450023.
- Cantwell, N., Owers, M., Meyers, J. and Riley, S. [2019] "Case studies on the application of passive seismic horizontal to vertical spectral ratio (HVSr) surveying for heavy mineral sand exploration," *ASEG Extended Abstracts* **2019**, 1–4.
- Combey, A., Mercerat, E. D., Díaz, J. E., Benavente, C. L., Perez, F. P., García, B., Palomino A. R. and Guevara, C. J. [2024] "Characterizing the seismic response and basin structure of Cusco (Peru): Implications for the seismic hazard assessment of a World Heritage Site," *Nat. Hazards* **121**, 2371–2396.
- Dobry, R., Borcherdt, R. D., Crouse, C. B., Idriss, I. M., Joyner, W. B., Martin, G. R., Power, M. S., Rinne, E. E. and Seed, R. B. [2000] "New site coefficients and site classification system used in recent building seismic code provisions," *Earthq. Spectra* **16**(1), 41–67.
- GB 50011 [2010] *Code for Seismic Design of Buildings* (The Ministry of Housing and Urban–Rural Development of the People's Republic of China, Beijing, China).
- General Affairs Bureau of Yokohama City (GABYC) [2019] "Strong motion network," <http://www.city.yokohama.lg.jp/somu/org/kikikanri/eq/>.

- Havenith, H. B. [2004] "Guidelines for the implementation of the H/V spectral ratio technique on ambient vibrations measurements, processing and interpretation," <https://hdl.handle.net/2268/250698>.
- Hayashi, Y., Morii, T., Onimaru, S. and Yoshikawa, M. [2003] "Study on ground amplification ratio in the calculation method of response and limit strength," *J. Struct. Constr. Eng.* **68** (567), 41–46.
- IBC [2012] *International Building Code* (International Code Council, Country Club Hill, Illinois, USA).
- Inoue, W., Hayashi, Y., Arai, H., Nakai, S. and Iiba, M. [2010] "A study on method to evaluate seismic amplification ratios of surface strata," *AIJ J. Technol. Des.* **16**(32), 107–112.
- Isari, M., Tarinejad, R., Foumani, R. S. and Ghalesari, A. T. [2023] "Evaluation the effects of wave scattering resonance from complex topographies using boundary element method," *J. Earthq. Tsunami* **17**(5), 2350018.
- Karimzadeh, S. and Askan Gündoğan, A. Y.Ş. E. G. Ü. L. [2024] "Simulation of strong ground motions from the October 30, 2020, Samos earthquake and validations against observed records, intensity distributions, and damages in İzmir, Türkiye," *J. Earthq. Tsunami* **18** (5), 2450015.
- Koyamada, K., Miyamoto, Y., Tokimatsu, K. and Miura, K. [2004] "Practical evaluation for soil response and pile stress in a liquefiable site using response spectrum method," *AIJ J. Technol. Des.* **19**, 47–52.
- Lam, N. T. K., Wilson, J. L. and Chandler, A. M. [2001] "Seismic displacement response spectrum estimated from the frame analogy soil amplification model," *Eng. Struct.* **23** (11), 1437–1452.
- Laouami, N. [2020] "Proposal for a new site classification tool using microtremor data," *Bull. Earthq. Eng.* **18**(10), 4681–4704.
- Li, Y. B., He, Y. Z., Liu, Y., Song, Q. S. L. and Xing, S. [2024] "Effect of site soil and bus bars on the seismic performance of an isolated power transformer," *J. Earthq. Tsunami* **18**(2), 2350039.
- Liu, G. H. and Li, X. Y. [2024] "Theoretically derived transfer functions and specific framework for simulating spatially varying seismic underground motions of media-transition site," *J. Earthq. Tsunami* **18**(3), 2350041.
- Liu, Z. X., Huang, Z. E., Huang, L., Sun, J. and Du, J. M. [2022] "Two-dimensional fast multipole indirect boundary element method-based solution to *P*-wave scattering by a mountain with large-scale random cracks in an elastic half-space," *J. Earthq. Tsunami* **16** (2), 2140007.
- Manakou, M., Roumelioti, Z. and Riga, E. [2023] "Shear-wave velocity determination by combining data from passive and active source field investigations in Kumamoto city, Japan," *Earth Planets Space* **75**(1), 163.
- Maringue, J., Sáez, E. and Yañez, G. [2021] "An empirical correlation between the residual gravity anomaly and the h/v predominant period in urban areas and its dependence on geology in andean forearc basins," *Appl. Sci.* **11**(20), 9462.
- Meng, Q. S., Li, Y., Wang, W. J., Chen, Y. H. and Wang, S. L. [2023] "A case study assessing the liquefaction hazards of silt sediments based on the horizontal-to-vertical spectral ratio method," *J. Mar. Sci. Eng.* **11**(1), 104.
- Midorikawa, M., Okawa, I., Iiba, M. and Teshigawara, M. [2003] "Performance-based seismic design code for buildings in Japan," *Earthq. Eng. Eng. Seismol.* **4**(1), 15–25.
- Miura, K., Koyamada, K. and Iiba, M. [2001] "Response spectrum method for evaluating nonlinear amplification of surface strata," *J. Struct. Eng.* **539**, 57–62.
- Morikawa, H. and Iiyama, K. [2021] "A method to find an appropriate input motion using a given motion on ground surface," *J. Earthq. Tsunami* **15**(1), 2150001.

- Moustafa, S. S., Abdalzaher, M. S., Khan, F., Metwaly, M., Elawadi, E. A. and Al-Arifi, N. S. [2021] "A quantitative site-specific classification approach based on affinity propagation clustering," *IEEE Access* **9**, 155297–155313.
- Nakamura, Y. [1989] "A method for dynamic characteristics estimation of subsurface using microtremor on the ground surface," *RTRI Q. Rep.* **30**(1), 25–33.
- Nakamura, Y. [1996] "Real-time information systems for seismic hazards mitigation UrEDAS, HERAS and PIC," *Q. Rep. RTRI* **37**(3), 112–127.
- Nakamura, Y. [2000] "Clear identification of fundamental idea of Nakamura's technique and its applications," in *Proc. 12th World Conf. Earthquake Engineering*, pp. 1–8.
- Ochiai, T., Inubushi, T. and Enomoto, T. [2019] "Creation of a hazard map considering regional characteristics by microtremor," *J. Jpn. Assoc. Earthq. Eng.* **19**(5), 5_136–5_145.
- Parla, R. and Somala, S. N. [2022] "Seismic ground motion amplification in a 3D sedimentary basin: Source mechanism and intensity measures," *J. Earthq. Tsunami* **16**(4), 2250008.
- Phung, V. B., Chang, Y. W., Loh, C. H., Huang, B. S., Ha, V. L., Nguyen, C. N. and Pham, D. H. [2024] "Regional and site-specific ground motion model for probabilistic seismic hazard analysis in Taiwan: A case study of I-Lan," *J. Earthq. Tsunami* **18**, 2450009, doi: 10.1142/S179343112450009X.
- Pranata, B., Yudistira, T., Saygin, E., Cummins, P. R., Widiyantoro, S., Brahmantyo, B. and Zulfakriza, Z. [2018] "Seismic microzonation of Bandung basin from microtremor horizontal-to-vertical spectral ratios (HVSr)," *AIP Conf. Proc.* **1987**(1), 020004.
- Rong, M. S., Wang, Z. M., Woolery, E. W., Lyu, Y. J., Li, X. J. and Li, S. Y. [2016] "Nonlinear site response from the strong ground-motion recordings in western China," *Soil Dyn. Earthq. Eng.* **82**, 99–110.
- Schnabel, P. B. [1972] "Shake, a computer program for earthquake response analysis of horizontally layered sites," *Report No. EERC 72-12, University of California, Berkeley*.
- Shi, L. J., Liu, J. X. and Chen, S. Y. [2022a] "Site classification based on predominant period of microtremor's H/V spectral ratio," *J. Vib. Shock* **41**(13), 34–42.
- Shi, Y., He, H. J. and Miao, Y. [2022b] "Multidirectional linear site response analysis by applying the SBSR technique to KiK-net data," *J. Earthq. Tsunami* **16**(2), 2140005.
- Sreejaya, K. P. and Raghukanth, S. T. G. [2022] "Hybrid broadband ground motion simulation for 2015 Mw 7.9 nepal earthquake," *J. Earthq. Tsunami* **16**(5), 2250015.
- Tsang, H. H., Chandler, A. M. and Lam, N. T. [2006a] "Simple models for estimating period-shift and damping in soil," *Earthq. Eng. Struct. Dyn.* **35**(15), 1925–1947.
- Tsang, H. H., Chandler, A. M. and Lam, N. T. [2006b] "Estimating non-linear site response by single period approximation," *Earthq. Eng. Struct. Dyn.* **35**(9), 1053–1076.
- Tsang, H. H., Wilson, J. L., Lam, N. T. K. and Su, R. K. L. [2017] "A design spectrum model for flexible soil sites in regions of low-to-moderate seismicity," *Soil Dyn. Earthq. Eng.* **92**, 36–45.
- View Wave [2019] "Real-time FFT spectrum analyzer system," <https://www.spectrasoft.jp>.
- Wen, P. and Bi, X. R. [2025] "Spatial variation analysis for ground motions based on regional site conditions and separation distance," *J. Earthq. Tsunami*, doi: 10.1142/S1793431125500034.
- Wen, P., Bi, X. R. and Luo, N. [2024] "Analysis of depth spatial variations of accelerograms recorded from the center for engineering strong motion data: Numerical simulation for multipoint ground motions," *J. Earthq. Tsunami* **19**, 2450029, doi: 10.1142/S1793431124500295.
- Wen, R. Z., Ji K., Ren Y. F. and Wang H. W. [2015] "Site classification for strong earthquake stations in China using spectral ratio method," *Chin. J. Rock Mech. Eng.* **34**(6), 1236–1241.
- Yu, Y. Y., Liu, Q. F. and Ding, H. P. [2023] "Sensitivity study of seismic amplification effect of large-scale Sichuan basin on key parameters during the great Wenchuan earthquake," *J. Earthq. Tsunami* **17**(6), 2350023.

- Yuliyanto, G. and Harmoko, U. [2019] "Identify the oil seepage in plantungan geothermal manifestation, Kendal using HVSr method," *E3S Web of Conf.* **125**, 15004.
- Zhang, H. Z., Saito, T. and Zhao, Y. G. [2017a] "Calculation method of seismic motion amplification ratio corresponding to fundamental period of layered soil profiles," *J. Struct. Eng.* **63B**, 343–349.
- Zhang, H. Z., Saito, T. and Zhao, Y. G. [2017b] "Simple calculation method of seismic motion amplification ratio corresponding to fundamental period," *J. Struct. Constr. Eng.* **82** (734), 597–604.
- Zhang, H. Z. and Zhao, Y. G. [2018a] "A simple approach for estimating the first resonance peak of layered soil profiles," *J. Earthq. Tsunami* **12**(1), 1850005.
- Zhang, H. Z. and Zhao, Y. G. [2018b] "Relationship between Fourier and response spectral ratios based on random vibration theory," in *Summaries of Technical Papers of Annual Meeting AIJ* (Tohoku), pp. 621–622.
- Zhang, H. Z. and Zhao, Y. G. [2019] "A simple approach for estimating the fundamental mode shape of layered soil profiles," *J. Earthq. Tsunami* **13**(1), 1950003.
- Zhang, H. Z. and Zhao, Y. G. [2021a] "Analytical model for response spectral ratio considering the effect of earthquake scenarios," *Bull. Earthq. Eng.* **19**(12), 5285–5305.
- Zhang, H. Z. and Zhao, Y. G. [2021b] "Investigation of relationship between the response and Fourier spectral ratios based on statistical analyses of strong-motion records," *J. Earthq. Tsunami* **15**(2), 2150008.